

12. PORE-FLUID TRACE METAL CONCENTRATIONS: IMPLICATIONS FOR FLUID/ROCK INTERACTIONS IN THE BARBADOS ACCRETIONARY PRISM¹

Yan Zheng² and Miriam Kastner³

ABSTRACT

Pore-fluid samples across the décollement zone at the northern Barbados accretionary prism were simultaneously analyzed at high resolution for their minor and trace element (Rb, Ba, Co, Zn, Mo) concentrations by inductively coupled plasma-mass spectrometry. Elevated Rb concentrations below the décollement zone suggest exchange with the oceanic basalt layer. The very different K/Rb concentration ratios across the décollement zone suggest that the fluids above and below this zone are geochemically distinct. Highly elevated concentrations of Mo, Zn, and Co, associated with a distinct Cl minimum depth interval at Site 948, imply that the source of this fluid is organic-rich sediment layers below the décollement zone, possibly the organic-rich turbidite layer encountered at Site 948. Ba concentrations are controlled largely by barite solubility equilibrium. The presence of Ba supersaturation within and immediately above the décollement zone at Site 948 and its absence at Site 949 is consistent with enhanced overpressuring at the latter site.

INTRODUCTION

It has long been recognized that overpressured pore fluids play an important role in long-distance transport of large blocks on subhorizontal faults (Hubbert and Rubey, 1959). Therefore, several novel geophysical experiments were conducted during Leg 156 to document and advance our understanding of the distribution and extent of fluid overpressuring and its relationship to fluid flow in the fine-grained, clay-rich northern Barbados accretionary prism and underthrust section. Sites 948 and 949 are located 4 km and 2 km west of the thrust front, and are representative of seismically positive and negative polarity décollement reflectors, respectively (Shipley et al., 1994). As part of the integrated scientific effort, high-resolution pore-fluid samples were obtained for chemical analyses across the décollement zone. The chemical composition of pore fluids provides important insights into fluid-flow patterns and fluid/rock interactions in accretionary prisms (Gieskes et al., 1989; Kastner et al., 1991).

Although the systematics of trace metal concentrations are often complicated and not very well understood, their affinity to different mineral phases and organic compounds changes as their carrier phases undergo diagenesis and metamorphism. The concentration changes are influenced mainly by mineral solubility equilibrium and diagenesis (both of which are dependent on pressure and temperature), as well as by advection and diffusion. Because this work represents the first attempt to simultaneously measure micromolar (μM) and nanomolar (nM) levels of a number of minor and trace elements (Rb, Ba, Co, Mo, and Zn) in small pore-fluid samples, we will summarize briefly the methodology used and the geochemical systematics of these metals in the results and discussion section. These data also supplement the wealth of information obtained from major element and isotope-ratio data for these fluids, and provide additional insights into the source, flow, and fluid-solid phase interactions at this segment of the Barbados accretionary complex.

METHOD

Pore-fluid samples were retrieved shipboard by squeezing in a titanium squeezer (Shipley, Ogawa, Blum, et al., 1995). To assess contamination, squeezing blanks were obtained by the same sampling procedure followed for sediment pore-fluid samples using ultra-deionized (Milli-Q) water of 18 M Ω . Sample splits returned to the Lamont-Doherty Earth Observatory were analyzed by inductively coupled plasma-mass spectrometry (ICP-MS; VG Plasma Quad2+), which is ideal for rapid and multi-element studies and is one of the most sensitive methods for inorganic analyses.

A method developed previously by Zheng to analyze pore-fluid samples recovered during Ocean Drilling Program Leg 141 was used. Counts were collected on individual isotopes that were chosen to minimize the isobaric interferences. Of the trace metals discussed in this paper, only Ba is subject to interference, from ¹³⁸La and ¹³⁸Ce, neither of which were abundant enough in the samples to significantly bias the results. Standards were prepared in 1:100 diluted Pacific surface seawater, which approximates the matrix of the sample solutions. In some pore-fluid samples, Ca concentrations were highly elevated relative to seawater concentration. To verify that this did not affect our analyses, several artificial matrices were made; the comparison between these artificial matrices and the surface seawater matrix showed no significant difference.

To correct for long-term drift of the machine, internal standards In and Tl were employed for the pulse counting mode and Sc was employed for the analog mode. Standards were run frequently between samples (approximately every five samples) to ensure the quality of the data. Leg 156 samples were analyzed after six months of storage. During this time, there was no significant evaporation, as indicated by the good agreement between the ICP-MS and shipboard Ca, Mg, Li, and Mn data (Tables 1, 2; Fig. 1). The overall precision (1σ as determined by 5 replicates of same sample) for each element analyzed was ~2%–5%, except for Zn, Cu, As, Ag, which could be as high as 15%.

RESULTS AND DISCUSSION

The shore-based metal results are given in Tables 1 and 2 for Sites 948 and 949, respectively, and are plotted vs. burial depth in Figures 2–8.

¹Shipley, T.H., Ogawa, Y., Blum, P., and Bahr, J.M. (Eds.), 1997. *Proc. ODP, Sci. Results, 156*: College Station, TX (Ocean Drilling Program).

²Lamont-Doherty Earth Observatory, Department of Earth and Environmental Sciences of Columbia University, Palisades, NY 10964, U.S.A. yzheng@ldeo.columbia.edu

³Scripps Institution of Oceanography, University of California, San Diego, 9500 Gilman Drive, La Jolla, CA 92093-0212, U.S.A.

Table 1. Interstitial water trace metal data, Hole 948C.

| Analytical method: | | Titrm | ICP-MS | Titrm | ICP-MS | IC | AES | ICP-MS | AAS | ICP-MS | ICP-MS | ICP-MS | ICP-MS | ICP-MS | ICP-MS | ICP-MS | ICP-MS | ICP-MS | |
|---------------------------------|-----------------|------------|------------|------------|------------|-------------------------|------------------|------------------|------------------|------------------|------------|------------------|------------------|------------|------------------|------------------|------------|------------|--|
| Core, section, interval (cm) | Depth (mbsf) | Ca (mM) | Ca (mM) | Mg (mM) | Mg (mM) | SO ₄ (mM) | Li (μ m) | Li (μ m) | Mn (μ m) | Mn (μ m) | Rb (nM) | Ba (μ m) | Mo (μ m) | Co (nM) | Zn (μ m) | Cu (μ m) | As (nM) | Ag (nM) | |
| 156-948C- | | | | | | | | | | | | | | | | | | | |
| 2X-4 130-150 | 426.7 | 42.8 | 42.2 | 19.8 | 21.4 | 15.3 | 50.8 | 45.9 | 65.5 | 63.6 | 158 | 1.29 | 1.09 | 111 | 15 | 8.3 | 792 | 169 | |
| 3X-5 120-150 | 437.9 | 43.1 | 42.0 | 19.2 | 20.0 | 16.0 | 56.4 | 49.6 | 63.2 | 59.3 | 169 | 1.82 | 0.94 | 58 | 5 | 6.3 | 821 | ND | |
| 4X-5 110-150* | 447.4 | - | - | - | - | - | - | - | - | - | - | - | - | - | - | - | - | - | |
| 5X-2 120-150# | 452.7 | 44.2 | 43.8 | 20.3 | 21.3 | 15.9 | 65.6 | 64.5 | 93.4 | 90.6 | 171 | 1.45 | 0.85 | 76 | 16 | 9.2 | 887 | 124 | |
| 6X-4 118-150# | 465.2 | 43.6 | 46.5 | 18.8 | 22.1 | 16.2 | 82.6 | 73.4 | 123.8 | 113.6 | 158 | 1.49 | 1.17 | 54 | 22 | 11.6 | 818 | ND | |
| 7X-6 120-150 | 477.8 | 45.3 | 46.4 | 18.5 | 19.6 | 15.0 | 80.8 | 71.1 | 139.6 | 126.3 | 125 | 2.68 | 1.48 | 75 | 45 | 17.9 | 731 | ND | |
| 8X-3 110-150# | 483.0 | 44.7 | 43.4 | 14.4 | 16.3 | - | 69.6 | 64.8 | 137.6 | 131.6 | 140 | 1.33 | 1.52 | 73 | 21 | 8.9 | 756 | ND | |
| 8X-6 120-150 | 487.6 | 46.3 | 47.6 | 16.2 | 19.1 | 14.4 | 80.7 | 69.7 | - | 132.9 | 134 | 2.83 | 1.51 | 71 | 21 | 9.2 | 748 | ND | |
| 9X-4 115-150 | 494.2 | 42.5 | 42.9 | 18.7 | 20.6 | 13.9 | 107.0 | 99.0 | 207.5 | - | 157 | 2.25 | 1.99 | 174 | 74 | 13.9 | 701 | ND | |
| 10X-3 110-150 | 502.4 | 42.3 | 42.7 | 24.1 | 26.6 | 14.2 | 177.8 | 148.8 | 611.6 | - | 252 | 1.69 | 1.10 | 235 | 36 | 10.3 | 950 | 167 | |
| 11X-3 120-150 | 512.1 | 42.4 | 39.8 | 31.5 | 30.0 | 14.8 | 215.2 | 150.7 | 440.5 | - | 243 | 2.35 | 0.60 | 137 | 76 | 15.8 | 814 | 267 | |
| 12X-4 110-150# | 523.2 | 42.2 | 45.5 | 33.2 | 36.5 | 14.1 | 173.6 | 147.2 | 142.0 | 117.4 | 272 | 1.37 | 0.91 | 155 | 21 | 7.8 | 817 | ND | |
| 13X-4 115-150 | 532.6 | 42.6 | 43.0 | 34.3 | 35.1 | 13.8 | 188.2 | 177.3 | 89.2 | 93.8 | 221 | 2.03 | 0.94 | 125 | 3 | 3.9 | 912 | ND | |
| 14X-3 110-150* | 540.4 | - | 44.3 | - | 36.9 | - | - | 181.4 | - | 70.1 | 154 | 1.65 | 0.53 | 154 | 9 | 5.5 | 825 | 476 | |
| 14X-5 120-150# | 543.5 | 44.0 | 44.3 | 35.7 | 36.1 | 13.0 | 170.0 | 173.6 | 57.9 | 54.5 | 302 | 2.22 | 0.68 | 110 | 15 | 12.9 | 770 | 263 | |
| 15X-6 110-150 | 554.2 | 43.1 | - | 37.5 | - | 11.9 | 242.6 | 225.2 | 51.0 | 52.6 | 263 | 2.44 | 0.45 | 144 | 7 | 13.1 | 641 | ND | |
| 16X-2 110-150 | 557.1 | 44.9 | 45.8 | 37.1 | 37.7 | 11.9 | 244.3 | 221.9 | 37.5 | 40.9 | 223 | 1.59 | 0.40 | 145 | 13 | 7.3 | 792 | 277 | |
| 17X-2 120-150# | 567.0 | 45.7 | 46.0 | 35.6 | 36.1 | 11.7 | 251.4 | 224.3 | 30.6 | 24.8 | 308 | 1.77 | 0.32 | 132 | 6 | 5.2 | 732 | ND | |
| 17X-5 000-040* | 570.3 | 48.5 | 49.4 | 37.6 | 37.7 | 10.7 | 273.6 | 242.4 | 32.4 | 32.4 | 264 | 2.05 | 0.42 | 221 | 4 | 4.2 | 708 | ND | |
| 18X-4 110-150 | 579.1 | 48.7 | 47.5 | 35.3 | 35.0 | 9.8 | 283.7 | 243.5 | 26.2 | 20.9 | 352 | 1.68 | 0.33 | 214 | 7 | 8.2 | 680 | ND | |
| 19X-4 110-150 | 588.6 | 51.1 | 51.0 | 35.4 | 35.9 | 10.2 | 302.8 | 262.9 | 22.6 | 26.6 | 276 | 3.06 | 0.71 | 282 | 11 | 13.0 | 697 | 140 | |

Notes: * = He sample excess interstitial water. # = squeezed after sealing and up to 24 hr storage in refrigerator. ND = not detected.

Table 2. Interstitial water trace metal data, Site 949.

| Analytical method: | | Titrm | ICP-MS | Titrm | ICP-MS | IC | AES | ICP-MS | AAS | ICP-MS | ICP-MS | ICP-MS | ICP-MS | ICP-MS | ICP-MS | ICP-MS | ICP-MS | ICP-MS | |
|---------------------------------|-----------------|------------|------------|------------|------------|-------------------------|------------------|------------------|------------------|------------------|------------|------------------|------------------|------------|------------------|------------------|------------|------------|--|
| Core, section, interval (cm) | Depth (mbsf) | Ca (mM) | Ca (mM) | Mg (mM) | Mg (mM) | SO ₄ (mM) | Li (μ M) | Li (μ M) | Mn (μ M) | Mn (μ M) | Rb (nM) | Ba (μ M) | Mo (μ M) | Co (nM) | Zn (μ M) | Cu (μ M) | As (nM) | Ag (nM) | |
| 156-949B- | | | | | | | | | | | | | | | | | | | |
| 1X-1, 120-150 | 245.5 | 37.7 | 37.6 | 32.4 | 32.1 | 16.5 | 59.5 | 53.8 | 82.3 | 93.2 | 209 | 1.07 | 0.70 | 125 | 13 | 9.1 | 415 | ND | |
| 2X-3, 0-40 | 257.0 | 38.0 | 37.4 | 32.6 | 32.5 | 16.1 | 68.0 | 61.9 | 131.1 | 110.8 | 212 | 1.79 | 0.67 | 1054 | 56 | 9.5 | 518 | ND | |
| 2X-5, 110-150 | 261.1 | 38.3 | 38.3 | 31.5 | 29.9 | 16.3 | 73.0 | 72.5 | 132.5 | 157.7 | 196 | 1.13 | 0.74 | 116 | 12 | 8.2 | 555 | ND | |
| 3X-5, 110-150 | 270.8 | 38.2 | 37.8 | 31.6 | 29.6 | 15.8 | 81.0 | 76.3 | 148.5 | 149.8 | 191 | 1.13 | 0.72 | 423 | 14 | 14.2 | 619 | 771 | |
| 4X-1, 125-150 | 274.5 | 38.3 | 37.7 | 31.5 | 30.9 | 16.0 | 85.0 | 83.1 | 146.3 | 154.3 | 217 | 0.98 | 0.70 | 107 | 11 | 17.2 | 593 | ND | |
| 5X-2, 110-150* | 285.6 | - | - | - | - | - | - | - | - | - | - | - | - | - | - | - | - | - | |
| 5X-4, 110-150 | 288.6 | 38.1 | 37.2 | 30.6 | 29.5 | 16.0 | 89.0 | 85.0 | 195.4 | 190.9 | 209 | 0.76 | 0.82 | 117 | 30 | 20.3 | 589 | ND | |
| 7X-2, 110-150 | 304.9 | 37.7 | 38.0 | 27.5 | 26.5 | 17.4 | 39.0 | 34.8 | 72.8 | 83.6 | 193 | 0.90 | 0.56 | 68 | 4 | 14.6 | 604 | ND | |
| 7X-6, 110-150 | 310.9 | 38.2 | 37.8 | 27.7 | 26.8 | 17.1 | 39.0 | 37.3 | 94.7 | 113.9 | 246 | 0.99 | 0.61 | 227 | 7 | 21.2 | 541 | ND | |
| 13X-1, 110-150 | 351.5 | 39.0 | 38.3 | 29.7 | 28.3 | 16.2 | 72.0 | 71.0 | 112.1 | 118.4 | 228 | 0.95 | 0.66 | 89 | 16 | 9.3 | 436 | ND | |
| 14X-2, 0-40#* | 355.8 | - | - | - | - | - | - | - | - | - | - | - | - | - | - | - | - | - | |
| 14X-5, 110-150 | 358.6 | 38.5 | 37.9 | 30.3 | 29.9 | 16.4 | 82.0 | 83.1 | 128.1 | 116.8 | 199 | 1.02 | 0.62 | 127 | 22 | 14.5 | 399 | 378 | |
| 15X-2, 110-150 | 362.7 | 40.2 | 39.2 | 30.3 | 30.4 | 16.0 | 86.0 | 88.4 | 163.8 | 136.7 | 182 | 0.86 | 0.69 | 100 | 3 | 6.4 | 543 | ND | |
| 15X-5, 110-150 | 367.2 | 39.5 | 38.8 | 30.0 | 29.8 | 15.7 | 94.0 | 99.5 | 155.1 | 153.4 | 227 | 0.99 | 0.64 | 108 | 10 | 17.9 | 557 | ND | |
| 17X-CC, 2-8 | 378.6 | 43.0 | 41.0 | 34.4 | 31.2 | 15.2 | - | 119.9 | 176.6 | 156.5 | 326 | 2.18 | 14.39 | 279 | 39 | 14.9 | 288 | 291 | |
| 19X-2, 60-100 | 401.1 | 38.7 | 38.1 | 34.3 | 32.6 | 15.0 | 167.0 | 169.3 | 546.1 | 452.9 | 305 | 1.13 | 0.52 | 273 | 18 | 19.8 | 570 | ND | |
| 22X-2, 110-150* | 430.2 | - | - | - | - | - | - | - | - | - | - | - | - | - | - | - | - | - | |
| 22X-5, 110-150 | 434.7 | 37.8 | 37.3 | 32.3 | 34.6 | 14.0 | 190.0 | 201.3 | 228.1 | 230.6 | 314 | 1.08 | 0.97 | 168 | 13 | 12.0 | 81 | ND | |
| 25H-3, 110-150 | 460.7 | 41.6 | 39.1 | 36.0 | 33.7 | 12.3 | 207.0 | 203.1 | 56.8 | 59.1 | 292 | 1.06 | 0.53 | 74 | 3 | 10.0 | 421 | 234 | |
| 156-949C- | | | | | | | | | | | | | | | | | | | |
| 2R-CC, 5-10 | 415.0 | - | - | - | - | - | - | - | - | - | - | - | - | - | - | - | - | - | |
| 4R-1, 0-4 | 425.2 | - | 35.0 | - | 33.7 | - | - | 175.6 | - | 452.8 | 335 | 1.33 | 13.05 | 440 | 24 | 18.2 | 451 | 122 | |
| 6R-CC, 8-15** | 453.6 | - | 35.7 | - | 34.4 | 16.2 | - | 183.6 | - | 210.6 | 418 | 1.39 | 4.13 | 170 | 7 | 11.9 | 754 | ND | |
| 7R-1, 80-90 | 455.0 | - | 39.7 | - | 35.1 | 12.7 | - | 230.7 | - | 64.4 | 315 | 1.30 | 0.57 | 206 | 13 | 22.5 | 472 | ND | |

Notes: ND = not detected. * = He samples. # = some extra sample available. ** = contaminated by drill water. Sub-bottom depths for Core 949B-14X are "corrected" depths (see "Operations" section, Shipley, Ogawa, Blum, et al., 1995).

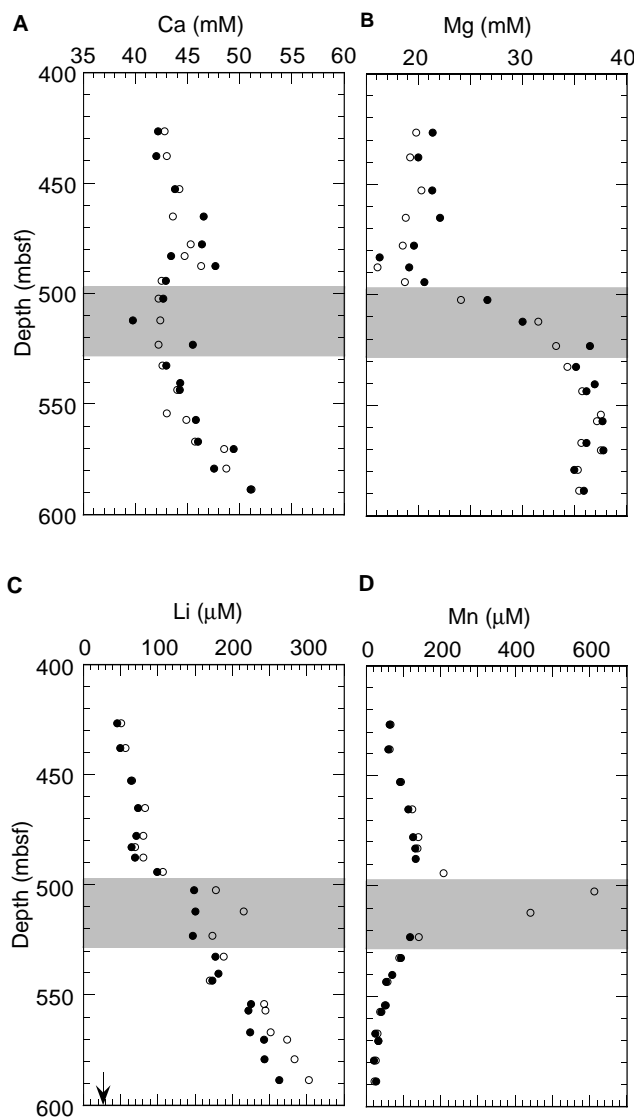


Figure 1. Concentration depth profiles, Site 948. **A.** Ca. **B.** Mg. **C.** Li. **D.** Mn. Arrow in (C) indicates seawater Li concentration. In all figures, open symbols are shipboard results (Shipley, Ogawa, Blum, et al., 1995) and solid symbols are ICP-MS results (except for Cl and K). Shaded area delineates décollement zone.

Site 948

Alkali Group (Li, Rb)

The concentration depth profile of Rb, along with the shipboard K and K/Rb data, are plotted in Figure 2. As with Li (Fig. 1C) and K (Fig. 2A), increased concentrations of Rb below the décollement zone indicate exchange with oceanic basalt layer II at moderate temperatures. The K/Rb value is considerably higher (~20) above the décollement zone than it is below it (~14). Two processes control the concentrations of the alkali elements in pore water. First, during moderate- to high-temperature basalt alteration, Li, K, and Rb are leached from the basalt or volcanic ash, resulting in enhanced concentrations of these elements in the solution (Staudigel and Hart, 1983; Berger et al., 1988). Second, at low temperatures the alteration products, mostly smectite, preferentially incorporate Cs>Rb>K>Na>Li because their energy of hydration increases from Cs to Li (Heier and Billings, 1970; Berger et al., 1988). Above the décollement zone, Li concentration is above the seawater value of 25 μM , whereas the K and Rb

concentrations are lower than the seawater values of 10.2 mM and 1.4 μM , respectively. This is a result of preferential incorporation of K and Rb over Li into mostly smectite. Below the décollement zone, the K and Rb concentrations increase but are still lower than the seawater values. This is most likely due to enhanced leaching from fresh basalt at higher temperature (Berger et al., 1988 and references therein) with a lesser extent of incorporation mostly into smectite. The difference in the K/Rb value across the décollement zone further indicates that the fluids above and below the décollement zone are chemically distinct.

Alkaline Earth Group (Ba)

Concentration depth profiles of Ba are plotted in Figure 3. Superimposed on the Ba concentration data is the calculated Ba saturation concentration based on pure barite equilibrium solubility as discussed below. The pore-fluid Ba concentrations are of the same order of magnitude as the barite Ba saturation concentration, suggesting an equilibrium solubility control. At some intervals, however, Ba concentrations are substantially supersaturated with respect to barite. Therefore, authigenic barite formation is expected at the in situ SO_4 concentrations, which, at all depths, are greater than 10 mM (Shipley, Ogawa, Blum, et al., 1995). Interestingly, barite crystals were observed in Mn carbonate veins from just above the décollement at Site 948 (Labaume et al., Chapter 5, this volume). ΔBa , defined as measured Ba concentration minus the calculated Ba saturation concentration with respect to barite, is plotted in Figure 3B. The significance of Ba supersaturation with barite will be discussed later.

Barite Solubility

Marine barite solubility is not only temperature and pressure dependent, but also a function of the ionic strength of the solution and the purity of the barite (Hanor, 1969; Church and Wolgemuth, 1972; Monnin and Galinier, 1988; Bertram, 1995). Laboratory experiments were performed at 1 atmospheric pressure (atm) to determine barite solubility in water. A thermodynamic approach was employed here to extend the calculation of barite solubility to the temperature and pressure range of interest for this study. The difficulty of thermodynamic calculations lies in determining the activity coefficients in the electrolyte solution. Ion-association models (Church and Wolgemuth, 1972) and ion-interaction models (also known as the Pitzer equation, see Monnin and Galinier, 1988; Bertram, 1995) have been used to estimate barite solubility in natural waters. Each of these complex models uses various assumptions, and the results vary somewhat (Bertram, 1995). The barite solubility product, $K_{sp}(1^\circ\text{C}, 500 \text{ atm})$, of the ion-interaction model is 40% smaller than of the ion-association model. For simplicity, we adopted a modified approach of the Church and Wolgemuth (1972) model.

The barite solubility product is defined as

$$K_{sp}(T,P) = a_{\text{Ba}} \times a_{\text{SO}_4} = \gamma_{\text{Ba}}^T m_{\text{Ba}} \times \gamma_{\text{SO}_4}^T m_{\text{SO}_4}, \quad (1)$$

where a is activity, γ^T is total ion activity coefficient, m is measured molality of the ion, and $K_{sp}(T,P)$ is a thermodynamic constant. The calculated $K_{sp}(T,P)$ values over the pressure and temperature range of interest for this study are listed in Table 3. The procedure used to obtain $K_{sp}(T,P)$ is as follows.

A best fit to the experimental data (Stephen and Stephen, 1963) of $K_{sp}(T, 1 \text{ atm})$ from 0°C to 100°C was utilized to calculate the solubility product at the temperatures of interest ($25^\circ\text{--}50^\circ\text{C}$) for which no experimental data were available. The fit was further adjusted by subtracting 0.3×10^{-10} to reproduce the $K_{sp}(25^\circ\text{C}, 1 \text{ atm})$ of 1.0×10^{-10} , used by Church and Wolgemuth (1972). This adjustment is based on the fact that most experimental data of inorganic barite solubility at 25°C have values of $(1.1 \pm 0.1) \times 10^{-10}$. An empirical

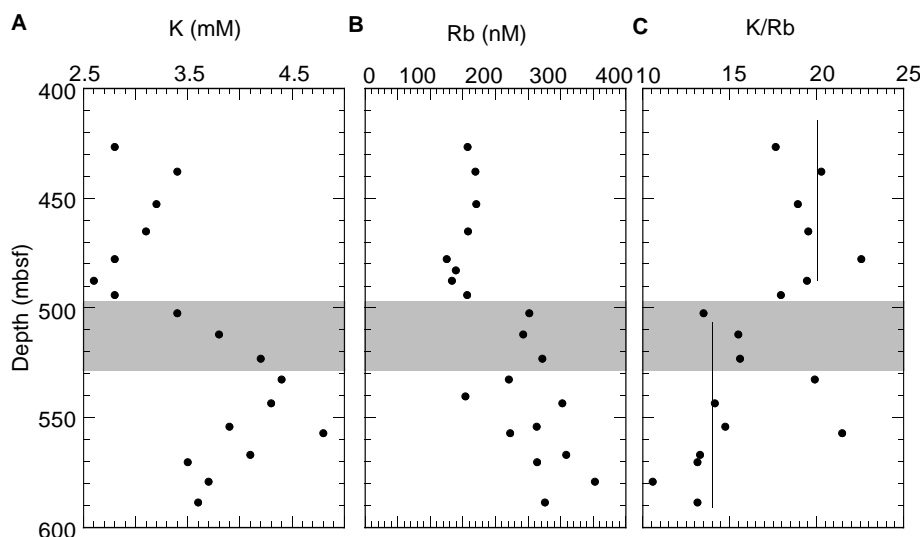


Figure 2. Concentration depth profiles, Site 948. **A.** K. **B.** Rb. **C.** K/Rb is expressed as 10^3 mol/mol. Lines are average K/Rb value.

formula for pressure dependence of mineral solubility in seawater (Millero, 1982; Eq. 1) was used to calculate $K_{sp}(T,P)$ from the molal volume and compressibility changes of Ba^{2+} , SO_4^{2-} , and BaSO_4 . The ionic strength of the pore water at Site 948 is 0.65 ± 0.04 and at Site 949 is 0.66 ± 0.01 . This is about 90% of the seawater ionic strength. All of the calculations here were based on seawater thermodynamic apparent constants and thus should be viewed as a close approximation. The temperature data are from shipboard temperature measurements (Shiple, Ogawa, Blum, et al., 1995) and pressure is calculated assuming hydrostatic pressure.

The effect of temperature and pressure on the single ion (Ba^{2+} and SO_4^{2-}) activity coefficient also has to be taken into account. For a single ion with an activity coefficient at 25°C and a pressure range of 500–700 atm, the following equation was used (Harned and Owen, 1958):

$$\frac{d \ln \gamma}{dP} = \frac{\Delta V(T)_{trans}}{2RT}, \quad (2)$$

where $\Delta V(T)_{trans}$ is the molal volume change for ions transferred from pure water to seawater (Millero, 1977) and R is the ideal gas constant. The right hand side of Equation 2 is on the order of 10^{-4} at 25°C and should not increase if the temperature varies from 25°C to 50°C . Therefore, the effect of temperature and pressure on the single ion (Ba^{2+} and SO_4^{2-}) activity coefficient is insignificant. Calculated values of 0.25 and 0.18 for 25°C and 500 atm were used for Ba^{2+} and SO_4^{2-} ion activity coefficients, respectively. Furthermore, SO_4^{2-} ion association pressure dependence was considered (Millero, 1971). The fraction of ions free of ion association, f , relates the single ion activity coefficient, γ , to the total ion activity coefficient γ^T by

$$\gamma^T = f \times \gamma. \quad (3)$$

SO_4^{2-} ion association with Na^+ , Ca^{2+} , and Mg^{2+} , using similar concentration of these elements in pore water, was calculated assuming there is no Cl^- ion association with these cations. It was found that for both Sites 948 and 949, the fraction of the SO_4^{2-} ion that is free of association is about 0.35 ± 0.1 at temperature ($25^\circ\text{--}45^\circ\text{C}$) and pressure (520–550 atm) of interest. Assuming that the pressure dependence on Ba^{2+} ion association is also small, the same value of 0.93 (Church and Wolgemuth, 1972) at 1 atm was used.

In summary, the temperature and pressure effects on the single ion activity coefficient and on ion association were found to be insignif-

icant in this case. Therefore the Ba concentration at saturation with barite can be calculated from the following:

$$m_{Ba_{sat}} = K_{sp}(T,P) / 0.25 \times 0.93 \times 0.18 \times 0.35 \times m_{SO_4}. \quad (4)$$

Impure barite with Sr substitution generally has different solubility than pure barite (Hanor, 1969; Felmy et al., 1993). Barite of marine origin has Sr/Ba mole ratio on the order of 0.01–0.05 (Goldberg et al., 1969). At this low Sr/Ba ratio, the effect of Sr substitution on solubility of barite can be ignored (Felmy et al., 1993).

The uncertainty of calculating Ba saturation concentrations with respect to barite, based on Equation 4, mainly comes from the uncertainty of $K_{sp}(T,P)$. The in situ fluid pressure may be approaching lithostatic pressure based on logging-while-drilling results (Moore et al., 1995). This will result in a slight increase of $K_{sp}(T,P)$ by about 5%. The above calculations and conclusions are based on the ion-association model of electrolyte solution. The ion-interaction model would have provided lower $K_{sp}(T,P)$ values by as much as 40%, resulting in even higher ΔBa than shown in Figure 3B.

Metals Associated with Organic Matter Diagenesis (Mn, Mo, Co, Zn)

A recent review by Calvert and Pedersen (1993) summarized the geochemical behavior of minor and trace elements known to be associated with organic-rich rocks. During early diagenesis of organic matter at the sediment seawater interface, some elements (Cu, Cd, Ni, Zn) are precipitated where free dissolved sulfide is present without undergoing a valency change, whereas others (Cr, Mn, Mo, Re, U, V) undergo a change in valency and are either efficiently adsorbed onto solid surfaces or are precipitated under anoxic conditions. Under oxygenated bottom water, Co is released in the Mn oxide reduction zone and is trapped when Mn oxide reprecipitates (Shaw et al., 1990). Therefore, even under oxic depositional conditions, diagenesis of sediments containing high organic carbon (>1%) will consume oxygen and can generate a shallow suboxic and anoxic reduction zone in which trace metals can accumulate by precipitation or adsorption. Upon burial at greater depths, the organic matter undergoes bacterial or thermal decomposition, which may cause valency changes or desorption of some of the elements, thus modifying their concentration in the pore water.

The pronounced Cl minimum just above the décollement zone seems to be the major fluid conduit. At this depth, elevated concen-

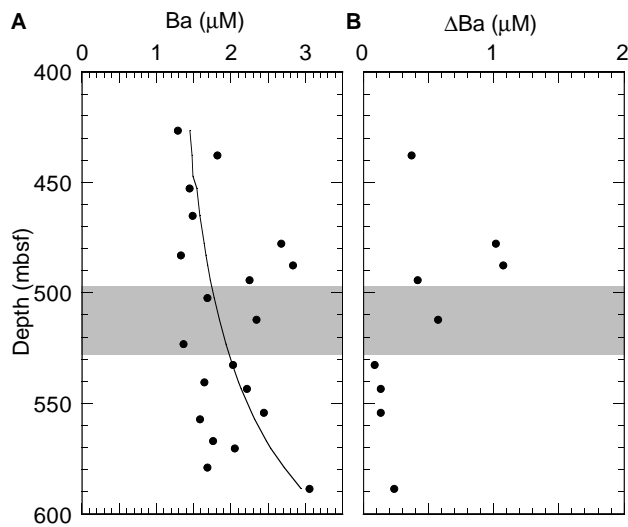


Figure 3. Concentration depth profiles, Site 948. **A.** Ba. **B.** Δ Ba ($Ba - Ba_{sat}$). Solid line is thermodynamically calculated Ba saturation concentration with respect to pure barite as explained in text. A second order polynomial fit of sulfate concentration with depth is used.

Table 3. Barite solubility constant K_{sp} (10^{-10}) in seawater as a function of pressure and temperature (see text for details of derivation).

| P (atm) | T (°C) | | | | | | |
|------------|--------|------|------|------|------|------|------|
| | 1 | 25 | 30 | 35 | 40 | 45 | 50 |
| 1 | 0.54 | 1.00 | 1.17 | 1.34 | 1.49 | 1.64 | 1.77 |
| 250 | 0.90 | 1.59 | 1.85 | 2.10 | 2.32 | 2.53 | 2.72 |
| 500 | 1.49 | 2.53 | 2.93 | 3.29 | 3.62 | 3.92 | 4.18 |
| 510 | 1.52 | 2.57 | 2.98 | 3.35 | 3.69 | 3.98 | 4.25 |
| 520 | 1.55 | 2.62 | 3.04 | 3.41 | 3.75 | 4.06 | 4.32 |
| 530 | 1.58 | 2.67 | 3.09 | 3.48 | 3.82 | 4.13 | 4.40 |
| 540 | 1.61 | 2.72 | 3.15 | 3.54 | 3.89 | 4.20 | 4.47 |
| 550 | 1.65 | 2.77 | 3.21 | 3.60 | 3.96 | 4.27 | 4.55 |
| 700 | 2.23 | 3.67 | 4.23 | 4.72 | 5.16 | 5.55 | 5.89 |

trations of Mn (Fig. 1D), Mo, Co, and Zn (Fig. 4) are observed. The extremely high concentration of Mn within the décollement zone is, however, related to local silica diagenesis, as discussed in the initial reports volume (Shipley, Ogawa, Blum, et al., 1995). A distinct maximum of Mo/Cl (not shown) coincides with the Cl concentration minimum. The most plausible source of Mn, Mo, Co, and Zn is the organic-rich gray to dark gray turbidite layer from below the décollement (Shipley, Ogawa, Blum, et al., 1995). The sediments above the décollement zone are extremely low in organic carbon content (<0.1wt%; Shipley, Ogawa, Blum, et al., 1995); therefore, the enriched Mn, Mo, Co, and Zn just above the décollement zone requires that the fluid must be generated deeper in the accretionary complex. If released at the depth of the thermogenic formation of hydrocarbons, these metals were mobilized and transported from an elevated temperature horizon at considerably greater burial depth. No direct data on the concentrations of these metals in the organic-rich gray to dark gray turbidite layer are available. Redox-sensitive elements (Mn, Fe, Cu, V, Zn, Sb, U) were reported to be enriched at the oxic/post-oxic boundary in similar North Atlantic turbidites (25°40'N, 30°57'W; Thomson et al., 1993).

Sulfate reduction, and hence sulfide production, intensifies below depths greater than 550 mbsf (Shipley, Ogawa, Blum, et al., 1995). The formation of sulfide is most likely responsible for the removal of Mo and Zn below the décollement zone, resulting in the lower observed concentrations of Mo and Zn below the décollement zone. In contrast, Co concentration is higher below the décollement zone, most likely because Co is not precipitated as sulfide.

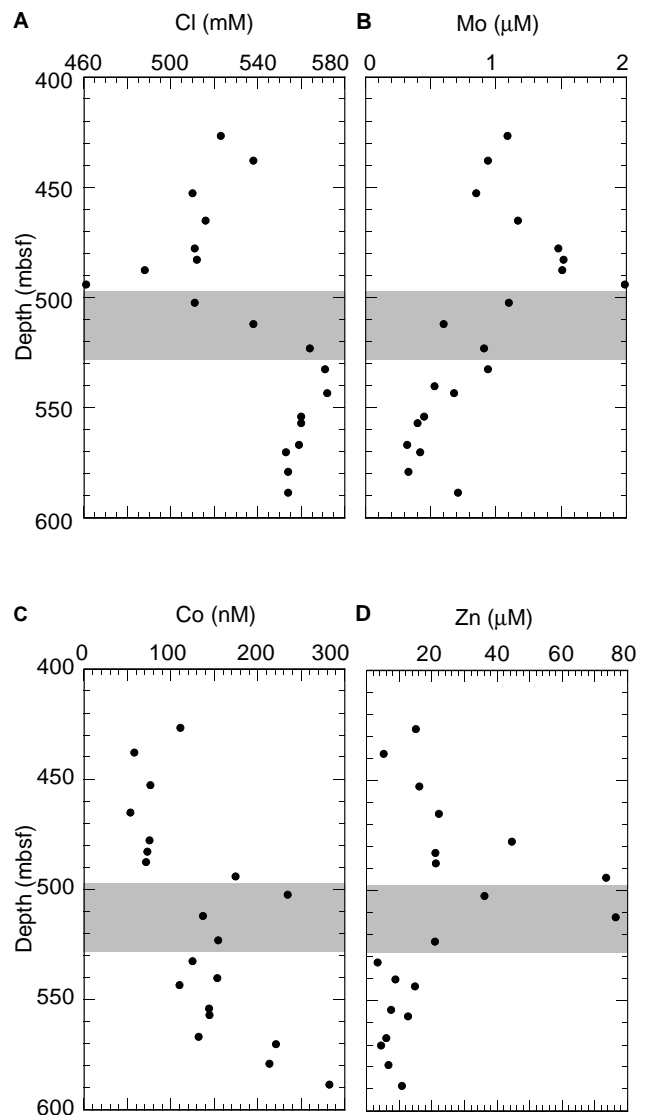


Figure 4. Concentration depth profiles, Site 948. **A.** Cl. **B.** Mo. **C.** Co. **D.** Zn.

Site 949

Alkali Group (Li, Rb)

Concentration depth profiles of Li, K, Rb and K/Rb ratio data are plotted in Figure 5. Both Li and Rb show increased concentrations below the décollement zone, indicating exchange with oceanic basalt layer II. The K/Rb ratio is higher (~20) above the décollement zone than below it (~12). Both Li and Rb display concentration ranges above and below the décollement zone similar to those at Site 948. The difference in the K/Rb ratio across the décollement zone is also similar to that at Site 948. In summary, a common origin of the fluids at both sites is clear.

Alkaline Earth Group (Ba)

Concentration depth profiles of Ca, Mg, Ba and Δ Ba are plotted in Figure 6. Shown with the Ba concentration data is the calculated Ba saturation concentration expected from pure barite equilibrium solubility. As with Site 948, Ba concentration appears to be controlled by the solubility of barite, although, with fewer data points above the saturation level compared to Site 948. Only at two depth intervals (257 and 378.6 mbsf) is substantial Ba supersaturation (Fig.

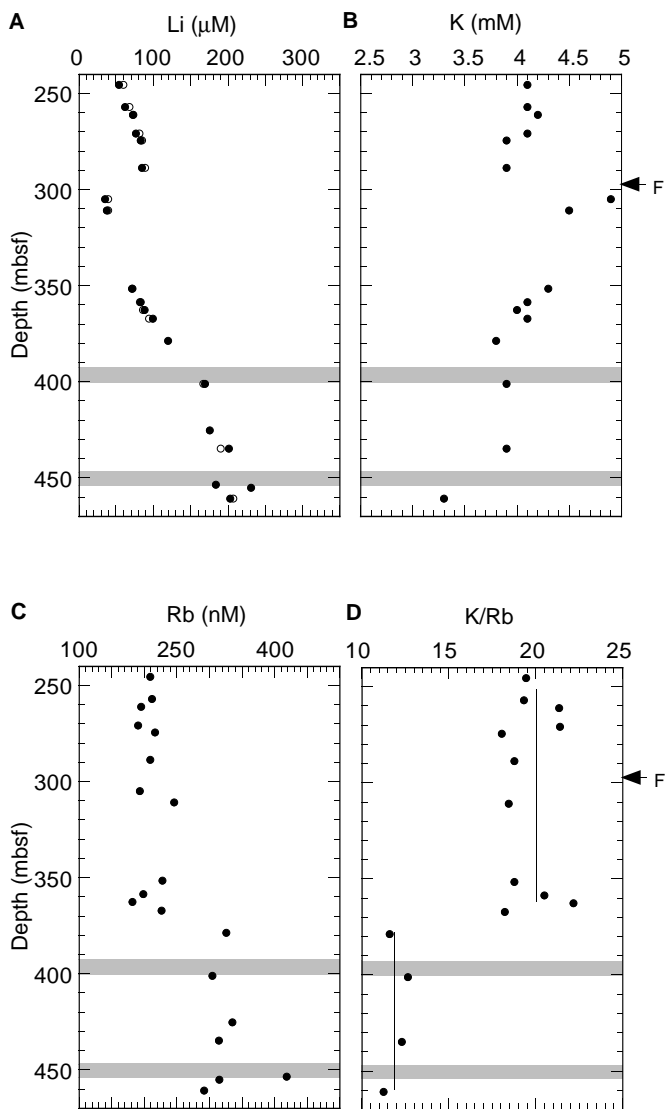


Figure 5. Concentration depth profiles, Site 949. **A.** Li. **B.** K. **C.** Rb. **D.** K/Rb expressed as 10^3 mol/mol. Lines are average K/Rb value. The arrow and *F* indicate the major thrust fault that was intercepted.

6D) with respect to barite observed, and thus authigenic barite formation is expected.

Metals Associated with Organic Matter Diagenesis (Mn, Mo, Co, Zn)

Concentration depth profiles of Cl, Mn, Mo, Co, Zn are plotted in Figures 7 and 8. Because the core recovery at Site 949 was poor (Shipley, Ogawa, Blum, et al., 1995), the profile of Cl is less continuous than that at Site 948. Site 949 is located closer to the thrust front of the accretionary prism; therefore, the freshening of pore water is not as pronounced as at Site 948. These two factors limited the usefulness of Cl concentrations alone as a tracer for fluid flow. At Site 948, fluid flow is characterized by low Cl concentrations along with enhanced concentrations of transition metals (Mn, Mo, Co, and Zn). This coincidence led us to believe that at Site 949 the elevated concentrations of Mn, Mo, Co, and Zn can be indicative of fluid source. For example, at a depth of ~434 mbsf, high concentrations of Mn, Mo, Co, and Zn were observed along with low Cl concentration (Fig. 7). At three other depth intervals (379, 425, and 454 mbsf) very high concentrations of Mo and elevated concentrations of Co, Zn, and Mn were also observed, but without distinguishable

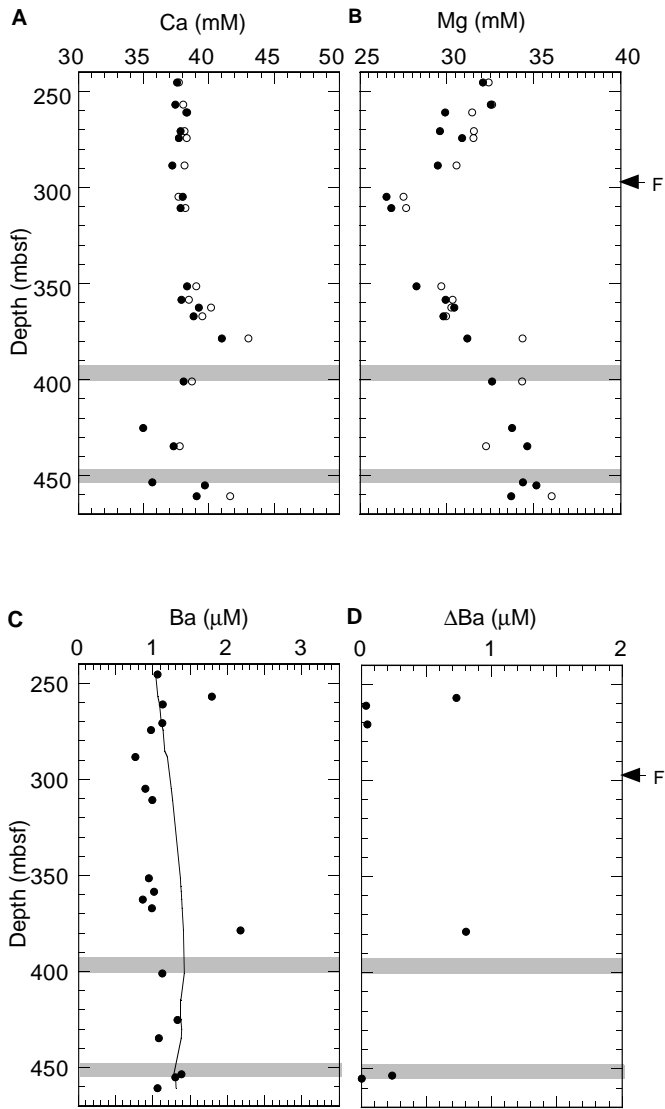


Figure 6. Concentration depth profiles, Site 949. **A.** Ca. **B.** Mg. **C.** Ba. **D.** Δ Ba ($Ba - Ba_{sat}$). Solid line is thermodynamically calculated Ba saturation concentration with respect to pure barite as explained in text. A second order polynomial fit of sulfate concentration with depth is used. The arrow and *F* indicate the major thrust fault that was intercepted.

Cl concentration reduction (Figs. 7, 8). These results also imply a common origin of fluids for both sites. The highest concentration of Mn, at a depth of 401 mbsf, is, however, a depositional feature related to silica cycling (Shipley, Ogawa, Blum, et al., 1995) and is not directly related to fluid generated from deep in the accretionary prism.

Speculation on Overpressuring and Fluid Flow

The observed difference of seismic polarity between Sites 948 and 949 décollement zones implies that the Site 949 décollement zone is more strongly overpressured compared to Site 948 (Shipley et al., 1994). Assessing the extent of fluid overpressuring and its relationship to fluid flow was one of the main goals of Leg 156. Two geochemical parameters obtained at Sites 948 and 949 allow speculations on the relative extent of overpressuring at Sites 948 and 949.

A dramatic freshening of the pore fluid and highly elevated concentrations of Mn, Mo, Co, and Zn were observed within or near the décollement zones at both sites. These observations strongly suggest

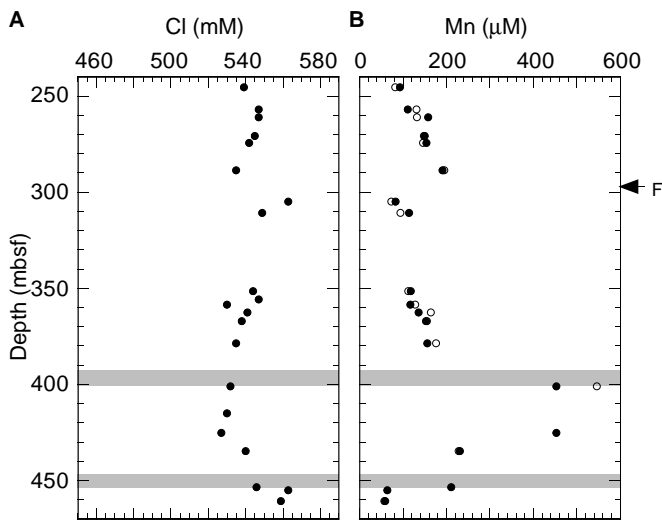


Figure 7. Concentration depth profiles, Site 949. **A.** Cl. **B.** Mn. The arrow and *F* indicate the major thrust fault that was intercepted.

that the fluids originated from deeper in the accretionary prism. However, the Ba saturation state, with respect to barite, is different at the décollement zones at Sites 948 and 949. Ba is supersaturated with respect to barite solubility at Site 948 in the upper part of the décollement zone and immediately above it where a major fluid conduit exists (Fig. 3B). In contrast, Ba is at equilibrium with respect to barite solubility at Site 949 (Fig. 6D). We invoke enhanced overpressuring at the Site 949 décollement zone to explain this difference.

Ba is leached from basalt, volcanic ash, and marine and terrigenous sediments during fluid/rock interactions at all temperatures. Ba is also especially enriched in organic matter and in siliceous marine sediments. It is removed mainly by barite precipitation. At both sites, sulfate is abundant; therefore, given time, the Ba concentration in the pore fluid should approach equilibrium values with respect to barite solubility, unless the pore water is controlled by other Ba input and output processes.

Characterized by low Cl, high Mn, Mo, Co, Zn, and Ba concentrations, the fluid generated deep in the accretionary prism moved into the décollement zones at both sites. This provided a continuous input of Ba into décollement zones at both sites. If the fluid flows at rates slower than that of barite precipitation, Ba will react with sulfate in the ambient pore water to form barite until the equilibrium value is reached. On the other hand, if there is continuous fluid flow transporting Ba at rates that exceed the barite precipitation rate, Ba concentration can deviate from that of the barite equilibrium solubility value. Accordingly, the supersaturated Ba concentration at the Site 948 décollement zone and immediately above it would be consistent with active fluid flow. Furthermore, the absence of Ba supersaturation with respect to barite solubility between 400 and 450 mbsf at the Site 949 décollement zone would indicate that barite precipitation outpaced fluid flow for Ba removal from the pore fluid. This would imply that the fluid flow is at a rate that is slower than the barite precipitation rate. If the apparent slow down of fluid flow at Site 949 is caused by the development of low permeability zones that inhibit escape of water during burial and deformation along the décollement, this would further imply enhanced overpressuring at this site.

The above scenario for Ba concentration control is supported by the following.

1. Barite is the only known chemical sink for Ba from the pore water.
2. Adequate thermodynamic calculation of barite solubility is utilized.

3. Barite precipitation (on the order of days or less) is a relatively slow process (Felmy et al., 1993). Therefore, Ba concentration of pore water has not been significantly lowered during coring and sampling.
4. Fluid flow is evident from the low Cl concentration horizon and elevated concentrations of Mn, Mo, Co, Zn, which could not have been produced locally.

However, we must caution that because of the poor recovery at this site, we do not know whether the clear conduit captured at Site 948 was possibly missed at Site 949. The Δ Ba at this interval is therefore unknown as well. This limited our ability to fully assess the influence of overpressuring on Ba chemistry.

CONCLUSIONS

Trace metal concentrations in the pore fluids from the northern Barbados accretionary prism are useful indicators of the fluid source and flow, consistent with other geochemical signals. They provide additional evidence that the fluids with low Cl concentrations are generated deep in the accretionary prism. The origin of the freshening of fluids is, however, not constrained by this study. At Site 948, Ba is supersaturated with respect to barite solubility equilibrium within and immediately above the décollement zone, but not at Site 949. Although not fully proven, this is consistent and may reinforce the conclusion of enhanced overpressuring in the décollement zone at Site 949 relative to Site 948, based on seismic data.

ACKNOWLEDGMENTS

We would like to thank Chieh Peng and Philip Rumford for their excellent technical support during Leg 156. The first author would also like to thank Dr. Philip N. Froelich for his encouragement to participate in the expedition. Discussion on barite solubility with Dr. M. Bertram was helpful. Discussions with ODP Leg 156 shipboard scientists during the cruise and post-cruise meeting are appreciated. The comments from two anonymous reviewers and the associate editor Dr. Jean Bahr have improved the quality of this paper significantly. This work was supported by the National Science Foundation through the United States Science Committee (JOI-USSAC) program to both authors.

REFERENCES

- Berger, G., Schott, J., and Guy, C., 1988. Behavior of Li, Rb and Cs during basalt glass and olivine dissolution and chlorite, smectite and zeolite precipitation from seawater: experimental investigations and modelization between 50° and 300°C. *Chem. Geol.*, 71:297–312
- Bertram, M.A., 1995. Benthic-biogeochemical responses to particle flux: The minerals and microbiota of Cross Seamount, (Ph.D. dissert.) University of Hawaii.
- Calvert, S.E., and Pedersen, T.F., 1993. Geochemistry of recent oxic and anoxic marine sediments: implications for the geological record. *Marine Geol.*, 113:67–88.
- Church, T.M., and Wolgemuth, K., 1972. Marine barite saturation. *Earth Planet. Sci. Lett.*, 15:35–44.
- Felmy, A.R., Rai, D., and Morre, A.D., 1993. The solubility of (Ba,Sr)SO₄ precipitates: thermodynamic equilibrium and reaction path analysis. *Geochim. Cosmochim. Acta*, 57:4345–4363.
- Gieskes, J.M., Blanc, G., Vrolijk, P., et al., 1989. Hydrogeochemistry in the Barbados accretionary complex: Leg 110 ODP. *Palaogeogr., Palaeoclimatol., Palaeoecol.*, 71:83–96.
- Goldberg, E.D., Somayajulu, B.L.K., Galloway, J., Kaplan, I.R., and Faure, G., 1969. Differences between barites of marine and continental origins. *Geochim. Cosmochim. Acta*, 33:287–289.
- Hanor, J.S., 1969. Barite saturation in sea water. *Geochim. Cosmochim. Acta*, 33:894–898.

- Harned, H.S., and Owen, B.B., 1958. *The physical chemistry of electrolytic solutions* (3rd ed.): New York (Rheinhold).
- Heier, K.S., and Billings, G.K., 1969. Lithium. In Wedepohl, K.H. (Ed.), *Handbook in Geochemistry*: New York (Springer-Verlag), 3B1–3O1.
- Hubbert, M.K. and Rubey, W.W., 1959. Role of fluid pressure in mechanics of overthrust faulting, I: mechanics of fluid-filled porous solids and its application to overthrust faulting. *Geol. Soc. Am. Bull.*, 70:115–166
- Kastner, M., Elderfield, H., and Martin, J.B., 1991. Fluids in convergent margins: what do we know about their composition, origin, role in diagenesis and importance for oceanic chemical fluxes? *Phil. Trans. R. Soc. London A*, 335:243–259.
- Millero, F.J., 1971. Effect of pressure on sulfate ion association in sea water. *Geochim. Cosmochim. Acta*, 35:1089–1098.
- , 1977. The use of specific interaction model to estimate the partial molal volume of electrolytes in seawater. *Geochim. Cosmochim. Acta*, 41:215–223.
- , 1982. The effect of pressure on the solubility of minerals in water and seawater. *Geochim. Cosmochim. Acta*, 46:11–22.
- Monnin, C., and Galinier, C., 1988. The solubility of celestite and barite in electrolyte solutions and natural waters at 25°C: A thermodynamic study. *Chem. Geol.*, 71:283–296.
- Moore, J.C., Shipley, T.H., Goldberg, D., Ogawa, Y., Filice, F., Fisher, A., Jurado, M.J., Moore, G.F., Rabaute, A., Yin, H., Zwart, G., Brückmann, W., Henry, P., Ashi, J., Blum, P., Meyer, A., Housen, B., Kastner, M., Labaume, P., Laier, T., Leitch, E.C., Maltman, A.J., Peacock, S., Steiger, T.H., Tobin, H.J., Underwood, M.B., Xu, Y., and Zheng, Y., 1995. Abnormal fluid pressures and fault-zone dilation in the Barbados accretionary prism; evidence from logging while drilling. *Geology*, 23:605–608.
- Shaw, T.J., Gieskes, J.M., and Jahnke, R.A., 1990. Early diagenesis in differing depositional environments: The response of transition metals in pore water. *Geochim. Cosmochim. Acta*, 54:1233–1246.
- Shipley, T.H., Moore, G.F., Bangs, N.L., Moore, J.C. and Stoffa, P.L., 1994. Seismically inferred dilatancy distribution, northern Barbados Ridge décollement: implications for fluid migration and fault strength. *Geology*, 22:411–414.
- Shipley, T.H., Ogawa, Y., Blum, P., et al, 1995. *Proc. ODP, Init. Repts.*, 156: College Station, TX (Ocean Drilling Program).
- Staudigel, H., and Hart, S.R., 1983. Alteration of basaltic glass: mechanisms and significance for the oceanic crust-seawater budget. *Geochim. Cosmochim. Acta*, 47:337–350.
- Stephen, H., and Stephen, T. (Ed.), 1963. *Solubilities of inorganic and organic compounds* (Vol. 1., Pt. 1): New York (Pergamon Press).
- Thomson, J., Higgs, N.C., Croudace, I.W., Colley S., and Hydes, D.J., 1993. Redox zonation of elements at an oxic/post-oxic boundary in deep-sea sediments. *Geochim. Cosmochim. Acta*, 57:579–595.

Date of initial receipt: 30 January 1996

Date of acceptance: 11 July 1996

Ms 156SR-021

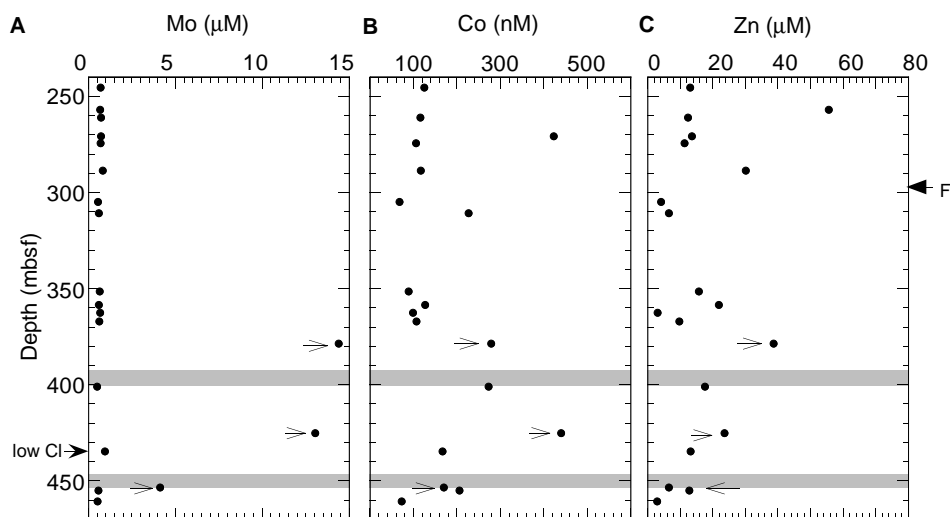


Figure 8. Concentration depth profiles, Site 949. A. Mo. B. Co. C. Zn. The simple arrows (→) indicate three depths where concentrations of Mn, Mo, Co, and Zn were all elevated. The arrow and F indicate the major thrust fault that was intercepted.